M&C 2017 - International Conference on Mathematics & Computational Methods Applied to Nuclear Science & Engineering, Jeju, Korea, April 16-20, 2017, on USB (2017)

Subcritical Copper-Reflected α-phase Plutonium (SCRαP) Measurements and Simulations

J. Hutchinson, R. Bahran, T. Cutler, W. Monange*, J. Arthur, M. Smith-Nelson, G. Caplin*, E. Dumonteil*

Los Alamos National Laboratory, P.O. Box 1663 P365, Los, Alamos, NM 87545
jesson@lanl.gov

**Institut de Radioprotection et de Sûreté Nucléaire (IRSN), PSN-EXP, SNC, Fontenay-aux-Roses 92262, France*

Abstract - *A Subcritical Copper-Reflected α-phase Plutonium (SCRαP) integral benchmark experiment has been designed and measured. The experiment design is discussed and preliminary results are presented. In the future this experiment will be evaluated and documented as a subcritical benchmark evaluation.*

I. INTRODUCTION

A Subcritical Copper-Reflected α-phase Plutonium (SCRαP) integral benchmark experiment has been designed and measured. In this experiment, multiplication is approximated using correlated neutron data from a detector system consisting of ^{3}He tubes inside high density polyethylene (HDPE). Measurements were performed on various subcritical experimental configurations consisting of a weapons-grade plutonium sphere surrounded by different Cu thicknesses. In addition to the proposed base experimental configurations with Cu, additional configurations were performed with the plutonium ball nested in various thicknesses of interleaved HDPE spherical shells mixed in with the Cu shells. The HDPE is intended to provide fast neutron moderation and reflection, resulting in additional measurements with differing multiplication, spectra, and nuclear data sensitivity.

The experiments were performed at the National Criticality Experiments Research Center (NCERC). A 4.5-kg α-phase stainless-steel clad plutonium sphere, referred to as the BeRP (Beryllium-Reflected Plutonium) ball due to its historical use in a beryllium-reflected critical experiment [1], was the plutonium core for this experiment. More detail on the physical characteristics of the BeRP ball can be found in a Reference [2].

In 2012, similar subcritical measurements were performed with the BeRP ball surrounded by nickel and tungsten. Both measurement sets were documented as benchmark evaluations and accepted by the International Criticality Safety Benchmark Evaluation Project (ICSBEP) [2,3].

Similar to past measurements, the proposed work will help identify deficiencies and quantify uncertainties in nuclear data, and validate computational methods related to neutron multiplication inference for subcritical benchmark evaluations.

II. EXPERIMENT DESIGN

1. Experiment information

A Solidworks® rendering of the preliminary design of the SCRαP integral benchmark experiment is shown in Fig. 1. The BeRP ball is surrounded by Cu hemishells as shown in Fig. 2. The assembly is built on an aluminum stand such that the center of the BeRP ball is at the same height as the center of the He-3 tubes of the multiplicity counter detector system, called the MC15.

Fig. 1. Preliminary Solidworks® Computer-Aided Design (CAD) rendering of the SCRαP integral experiment. The BeRP ball inside nested Cu is in the center. Two MC15 detector systems are used to estimate the multiplication of each configuration.

The experiment design consisted of the BeRP ball nested in various thicknesses of Cu spherical shells and interleaved polyethylene spherical shells. In total, 16 different configurations were designed: 1 bare configuration, 8 copper-reflected configurations (up to a maximum of 4 inches-thick) and 7 configurations with polyethylene and copper reflection (also up to a maximum

of 4 inches-thick). There are two purposes for the configurations with polyethylene: they allow for higher multiplication factor than with copper alone; and they allow for a different neutron spectra (and resulting sensitivity) for the same multiplication factor.

Fig. 2. Preliminary Solidworks® Computer-Aided Design (CAD) rendering of the SCRαP integral experiment. The BeRP ball can be seen in the center of the nested Cu (*bottom*) and Cu/polyethylene (*top*) shells.

The Cu alloy C101 was used for all of the hemishells. This alloy contains a minimum of 99.99 wt.% Cu. One of the Cu hemishells is shown in Fig. 3.

Fig. 3. A copper hemishell for use in the SCRαP experiment.

For this experiment, the MC15 multiplicity detector system was used. This detector consists of 15 He-3 tubes embedded in HDPE. The detector system records list-mode data (a time list of every recorded neutron event to a resolution of 128 nsec). Fig. 4 shows the MC15 detector system. For the SCRαP experiment, two MC15 systems were present and collected data in the same time list.

During the measurements, temperature data loggers were concurrently providing temperature data for the BeRP ball and its surroundings.

More information on the SCRαP experiment can be found in the final design documentation [4].

Fig. 4. Photograph and MCNP® model of the MC15 detector system.

2. Monte Carlo Simulation Results

The radiation transport tool used for the preliminary design simulations of the SCRαP integral benchmark experiment was the Los Alamos National Laboratory Monte Carlo N-Particle Code (MCNP®) version 6.1 [5]. MCNP® was used to determine the k_{eff} of different experimental configurations with increasing reflector thicknesses and material type. MCNP® was also

used to generate nuclear data sensitivities to each energy-dependent, nuclide-reaction-specific cross-section data component for k_{eff}. For the preliminary design, simplified MCNP® models were adopted that only incorporated the BeRP Ball, stainless steel cladding, and pure copper/polyethylene spherical reflectors. The evaluated nuclear data library adopted for the simulations was ENDF7.1 [6].

The simulated KCODE results of each configuration and sensitivity for the Cu-63 and Cu-65 cross-sections are shown in Fig. 5. During the preliminary design, this plot showed that at around 4 inches, the average sensitivity to the Cu total cross section no longer increases with additional Cu thickness. In addition, other issues arise at around this thickness (difficulty in handling the hemishells, criticality safety concerns, etc); for these reasons, a maximum thickness of 4 inches was chosen for this experiment.

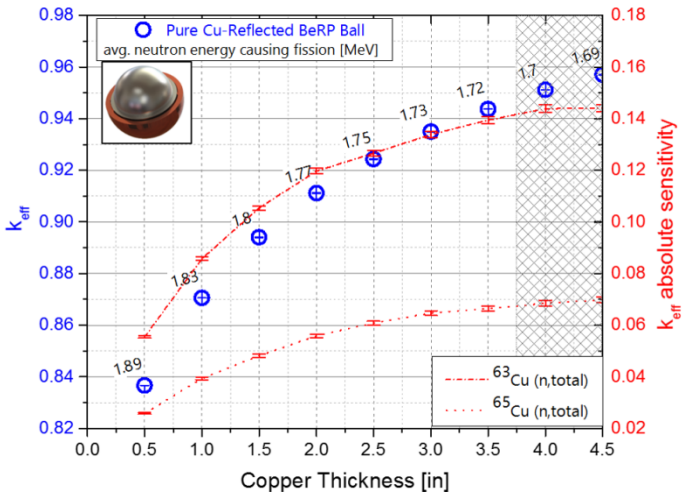

Fig. 5. MCNP® results for all Cu-reflected BeRP Ball base configurations highlighting the simulated k_{eff}, average neutron energy causing fission, and absolute copper total cross section sensitivity.

The k_{eff} absolute sensitivity for Cu-63 is shown in Fig. 6. A similar plot for Cu-65 will be shown at the meeting. These sensitivities have been compared to critical configurations in the ICSBEP handbook. It should be noted that there are a limited number of copper-reflected critical experiments in the handbook (8 experimental series with U fuel and 2 experimental series with Pu fuel). The maximum total Cu-63 sensitivity for the 16 subcritical configurations (0.143) is greater than the two Pu experimental series (0.126) but less than that for some of the U experimental series (0.200). In the intermediate energy regime, the maximum Cu-63 sensitivity for the 16 configurations (0.018) is greater than the two Pu experimental series by nearly an order of magnitude (0.002), but similarly less than that for some of the U experimental series (0.051). Similar results will be presented for Cu-65.

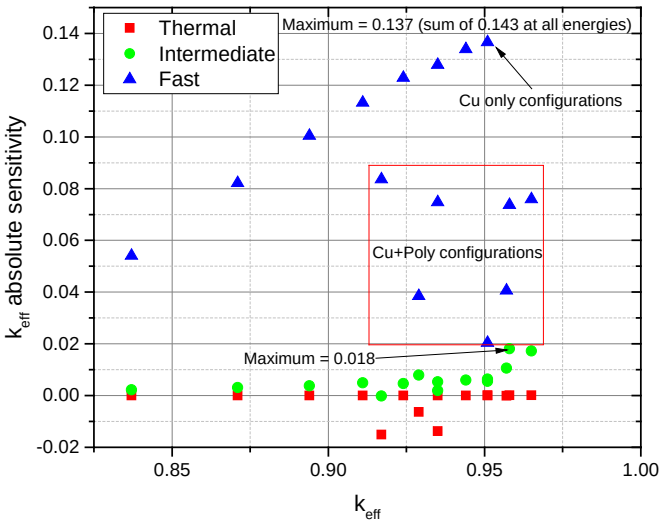

Fig. 6. k_{eff} sensitivity to Cu-63 as a function of k_{eff}.

The previous evaluated BeRP ball subcritical configurations (nickel and tungsten reflection) were used to predict some of the major experimental uncertainties that were be present for these measurements. A previous work shows that although simulations for subcritical experiments must be run in a different manner than critical experiments to allow for multiplicity analysis, criticality eigenvalue simulations can still be used to estimate experimental uncertainties for the primary subcritical benchmark parameters, allowing for tremendous savings in computational time (more than an order of magnitude on average) [7].

This method was used to estimate the experimental uncertainties for three benchmark parameters: detector singles count rate (R_1) i.e. the count rate in the detector system; the doubles count rate (R_2) i.e. the rate in the detector system in which two neutrons from the same fission chain are detected; and the leakage multiplication (M_L) i.e. the number of neutrons escaping a system per starter neutron. This was done for three different configurations; the results for one of these configurations (0.5 inch-thick HDPE surrounded by 3.5 inch-thick copper) is shown in Table I. It should be noted that the Cu mass was expected to be a minor uncertainty, which the table confirms.

Table I. Estimate of experimental uncertainties for Configuration 15 (0.5 inch-thick HDPE surrounded by 3.5 inch-thick copper).

Parameter	Experimental Uncertainty	Uncertainty
M_L	Pu radius ± 2 mils	0.18
	Pu isotopics ± 0.5%	0.19
	Cu thickness ± 0.3 cm	0.03
	Cu mass ± 0.5%	0.00006
R_1	Pu radius ± 2 mils	1024
	Pu isotopics ± 0.5%	1045
	Cu thickness ± 0.3 cm	141
	Cu mass ± 0.5%	0.34
R_2	Pu radius ± 2 mils	37450
	Pu isotopics ± 0.5%	41336
	Cu thickness ± 0.3 cm	5252
	Cu mass ± 0.5%	13.1

III. EXPERIMENT OVERVIEW

Seventeen different configurations were measured as shown in Table II. These included the 16 planned configurations and an additional configuration consisting of HDPE only. Additional information on these configurations is given in Table III; the simulations for the k_{eff} results in this table were performed during the experiment design with preliminary models. Fig. 7 shows configuration 7 during assembly. Fig. 8 shows the setup for the benchmark measurements. The two MC15 detector systems are connected together (for each measured file, a single file is created with 30 channels).

In order to determine the detector efficiency, Cf-252 source replace measurements were performed. These setup was identical to the benchmark configurations except a Cf-252 source was placed at the center of the assembly (instead of the Pu sphere) as shown in Fig. 9. An aluminum holder was made which places the source at the center of the inner-most hemishells for each configuration. The source strength of the Cf-252 source at the time of the measurements was 7.59e5 fissions/sec +/- 1.0%.

Table II. Hemishell layers which were present for each configuration. Orange represents Cu and light grey is used for HDPE. This pictorial color representation will be used in subsequent graph legends.

Configuration #	Layer number (each layer is 0.5 inches thick)							
	1	2	3	4	5	6	7	8
0								
1								
2								
3								
4								
5								
6								
7								
8								
9								
10								
11								
12								
13								
14								
15								
16								

Table III. Additional information on each configuration: total HDPE and Cu thickness and simulated k_{eff} values.

Configuration #	Thickness (inches)			Simulated k_{eff}	
	HDPE	Cu	HDPE+Cu	LANL	IRSN
0	0.0	0.0	0.0	0.774	0.777
1	0.0	0.5	0.5	0.837	0.829
2	0.0	1.0	1.0	0.871	0.862
3	0.0	1.5	1.5	0.894	0.884
4	0.0	2.0	2.0	0.911	0.900
5	2.0	1.0	3.0	0.917	0.907
6	0.0	2.5	2.5	0.924	0.914
7	2.0	2.0	4.0	0.929	0.921
8	2.0	2.0	4.0	0.935	0.919
9	0.0	3.0	3.0	0.935	0.923
10	0.0	3.5	3.5	0.944	0.933
11	0.0	4.0	4.0	0.951	0.939
12	1.5	2.0	3.5	0.951	0.939
13	1.0	2.5	3.5	0.957	0.943
14	0.5	3.0	3.5	0.958	0.942
15	0.5	3.5	4.0	0.965	0.948
16	4.0	0.0	4.0	-	-

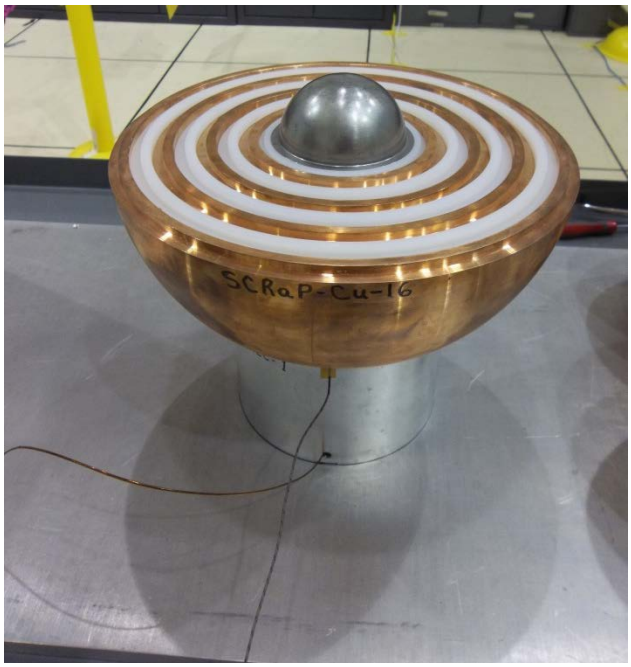

Fig. 7. Configuration 7 during assembly.

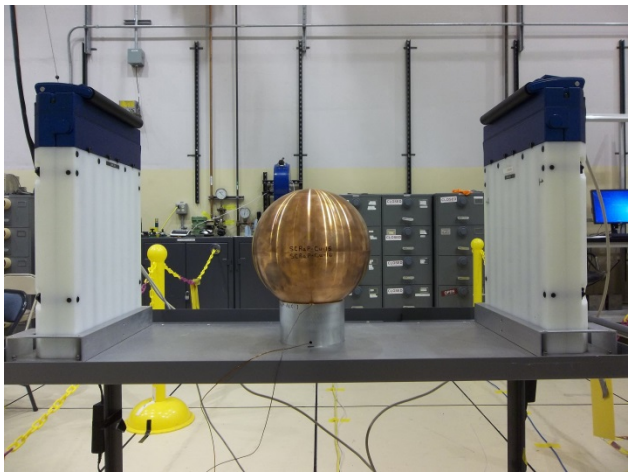
Fig. 8. Experimental setup for configuration 15.

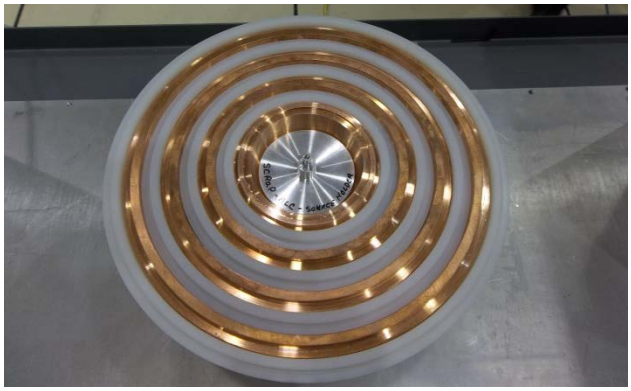
Fig. 9: Configuration 8 during assembly for Cf-252 measurements.

IV. PRELIMINARY RESULTS

As previously mentioned, the MC15 detector system records list-mode data. This is a list of every recorded neutron event (with a timing resolution of 128 nsec). These type of data can be analyzed using a variety of neutron multiplicity methods. Most of these noise analysis methods involve looking at time gates (anywhere from the low micro-second to milli-second range) and observing some quantity (such as the number of neutrons in each time gate or the number of time differences in each time gate). Many of these analysis methods have been used since the 1960s and are described in other works [8-9]. All results presented in this paper are preliminary; the final results will be published in the ICSBEP handbook.

One basic way to look at list-mode data is to create Feynman histograms [10]. In order to construct a Feynman histogram, one simply goes through a measured file with a fixed gate-width time (τ) and determines the number of recorded events in each gate. The number of gates which recorded "n" events is referred to as C_n. The total counting time is equal to:

$$Time = \tau \sum C_n \qquad (1)$$

It should be noted that there are multiple ways that one can bin data when constructing Feynman histograms; for this work the basic sequential method was used [11].

Fig. 10 shows Feynman histograms for a subset of the measured configurations (configurations 6-11). As the multiplication of a system increases, the observed histogram deviates more from a Poisson distribution (solid lines). It can easily be seen that for the pure copper systems, both the Poisson and Feynman histograms are moving to the right (they have more neutrons per gate).

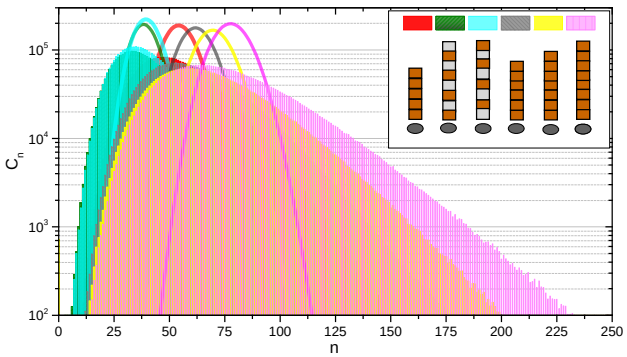

Fig. 10. Feynman histograms for configurations 6-11 with a gate-width of 1024 micro-sec.

After obtaining Feynman histograms, one can calculate the system multiplication using a system of

equations. For this work, the Hage-Cifarelli formalism was used [12].

After preparing Feynman histograms, reduced factorial moments are calculated using the equation:

$$m_r(\tau) = \frac{\sum_{n=0}^{\infty} n(n-1)\cdots(n-r+1)\,p_n(\tau)}{r!} \quad (2)$$

where $p_n(\tau)$ is the normalized fraction of gates that recorded n events:

$$p_n(\tau) = \frac{C_n(\tau)}{\sum_{n=0}^{\infty} C_n(\tau)} \quad (3)$$

Note that the count rate (as called the singles count rate or R_1) can be calculated using the equation:

$$R_1(\tau) = \frac{m_1(\tau)}{\tau} \quad (4)$$

Fig. 11 shows the count rate of the benchmark measurements (with the BeRP ball) and the detector efficiency (measured using Cf-252 replacement measurements). The efficiency is simply defined as the ratio of the count rate (R_1) of the replacement measurements divided by the reported neutron emission rate:

$$\varepsilon = \frac{R_1(\tau)}{F_S \bar{\nu}_{S(1)}} \quad (5)$$

where F_S is the reported spontaneous fission emission rate of the Cf-252 source, $\bar{\nu}_{S(1)}$ is the average number of neutrons emitted per Cf-252 fission, and R_1 is the detector count rate for the Cf-252 measurement (not the Pu measurement). These two parameters are plotted together to show that the reason that the count rate goes down significantly for the configurations with HDPE is due to the decrease in efficiency (which is caused by neutron absorption primarily in the hydrogen).

It should also be pointed out that for the pure copper cases (such as configurations 0-4 or 9-11) the slope of the count rate is much sharper than the increase in detector efficiency. This is because the detector count rate is proportional to both efficiency and system multiplication.

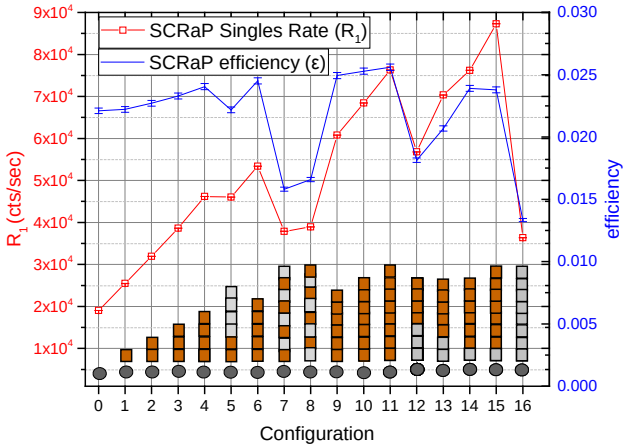

Fig. 11. Count rate (R_1) and detector efficiency (ε) for SCRαP configurations.

The excess variance (deviation of a Feynman histogram from a Poisson distribution) is proportional to Y_2, given by:

$$Y_2(\tau) = \frac{m_2(\tau) - \frac{1}{2}[m_1(\tau)]^2}{\tau} \quad (6)$$

This parameter is shown for all of the Cu-only configurations in Fig. 12. As expected, the amount of excess variance increases with Cu thickness (due to an increase in the system multiplication).

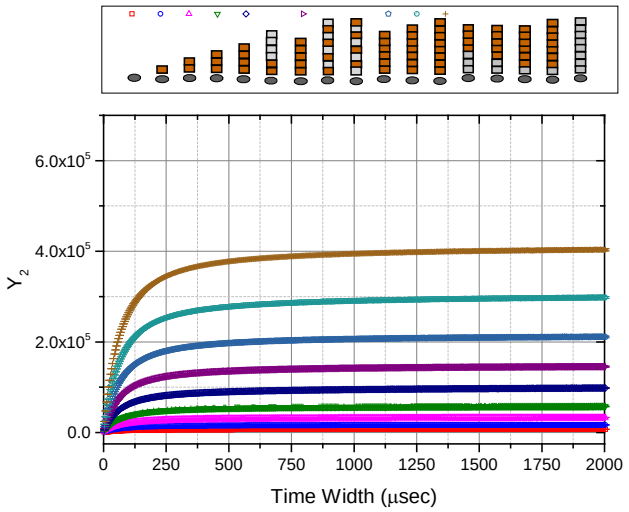

Fig. 12. Y_2 for Cu-reflected configurations.

A fit can be performed on the Y_2 curves to calculate the neutron lifetime/slowing-down time (1/λ) using the equation:

$$\omega_2(\lambda,\tau) = 1 - \frac{1-e^{-\lambda\tau}}{\lambda\tau} \tag{7}$$

Note that the MC15 detector system has a slowing-down time of around 35 micro-seconds (this is the time for neutrons to slow down in the HDPE present in the detector system prior to absorption in the He-3). Therefore the true lifetime is not being measured for fast systems. For this experiment, the lifetime/slowing-down time is shown in Fig. 13. It can be seen that for the configurations with Cu only, the result is approximately 35 micro-seconds as expected, but it is significantly larger for the configurations that include HDPE hemishells.

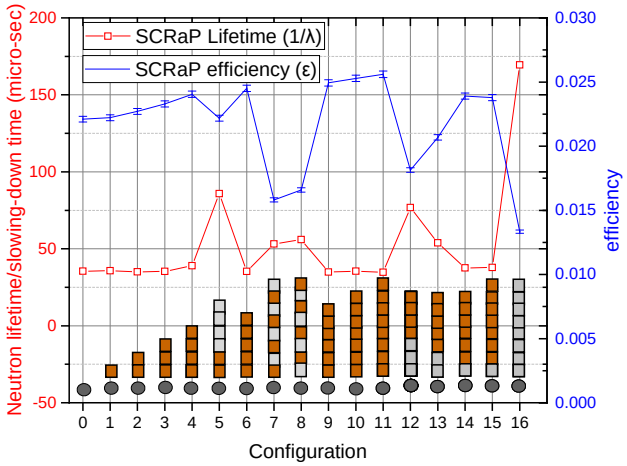

Fig. 13. Neutron lifetime/slowing-down time.

After determining the lifetime/slowing-down time, one can calculate the doubles counting rate (R_2) using Eq 8. This is the rate at which two neutrons from a single fission chain is detected. Fig. 14 shows the doubles counting rate for all of the configurations.

$$R_2(\tau) = \frac{Y_2(\tau)}{\omega_2(\lambda,\tau)} \tag{8}$$

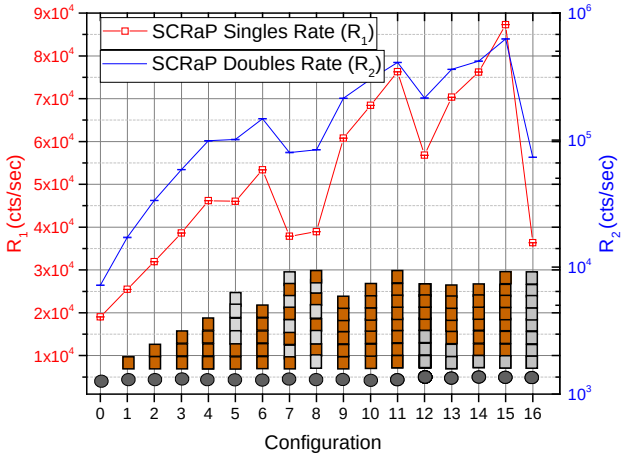

Fig. 14. Doubles counting rate (R_2).

If one assumes that there is no (α,n) neutron emission (a valid assumption for a fast metal system), then the system leakage multiplication, M_L, can be calculated using:

$$M_L = \frac{-C_2 + C_4}{2C_1}$$

with

$$C_1 = \frac{\bar{\nu}_{S(1)}\bar{\nu}_{I(2)}}{\bar{\nu}_{I(1)} - 1}$$

$$C_2 = \bar{\nu}_{S(2)} - \frac{\bar{\nu}_{S(1)}\bar{\nu}_{I(2)}}{\bar{\nu}_{I(1)} - 1} \tag{9}$$

$$C_3 = -\frac{R_2(\tau)\bar{\nu}_{S(1)}}{R_1(\tau)\varepsilon}$$

$$C_4 = \sqrt{C_2^2 - 4C_1C_3}$$

The terms $\bar{\nu}_{S(1)}$, $\bar{\nu}_{S(2)}$, $\bar{\nu}_{I(1)}$, and $\bar{\nu}_{I(2)}$ are the first and second factorial moments of the P_ν distribution where S refers to the isotope producing spontaneous fission neutrons and I refers to the isotope undergoing induced fission.

The leakage multiplication is shown for all of the configurations in Fig. 15. Appendix L of Reference 3 provides the equations that relate M_L to the multiplication factor (k_{eff}).

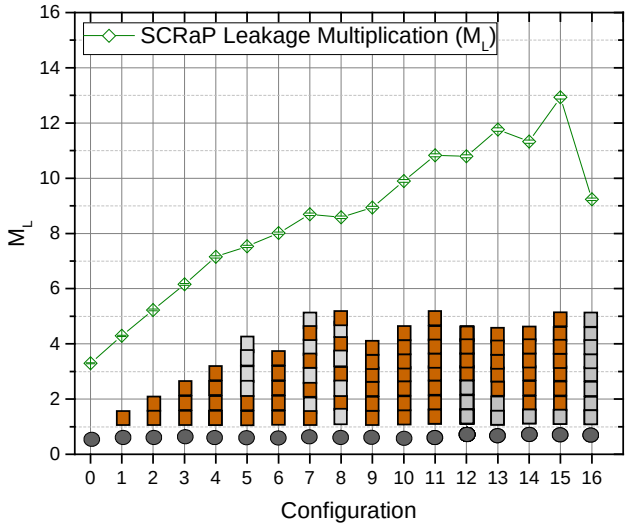

Fig. 15. Inferred leakage multiplication (M_L).

During the experiment design, the k_{eff} of each configuration was simulated using MCNP6 and MORET [13]. The leakage multiplication was calculated from the multiplication factor using basic equations with assumptions for the delayed neutron fraction. The MCNP models were simplified models (perfect spherical reflectors with no materials present outside the reflectors) but the MORET models had additional details (MC15 detectors, detailed reflector hemishells, etc.). It can be seen in Fig. 16 that the MORET results compare much better to the measured results than the MCNP simulations. In the future this will be investigated in detail. The (C/E)/E between the simulated IRSN results and the measured results are shown in Fig. 17.

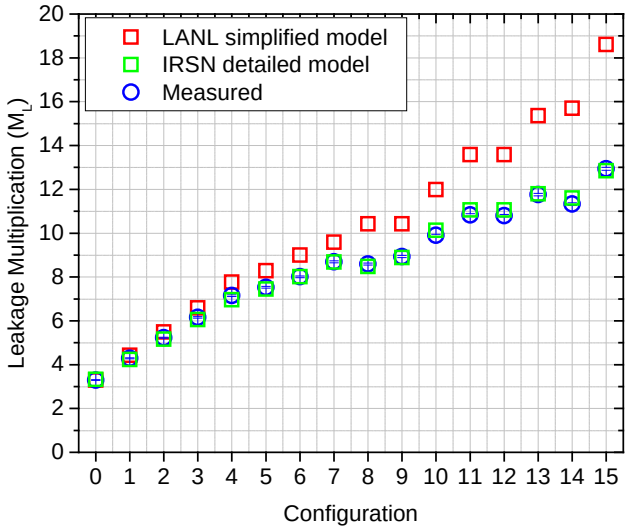

Fig. 16. Comparison of measured leakage multiplication to simulations in MCNP (performed by LANL) and MORET (performed by IRSN).

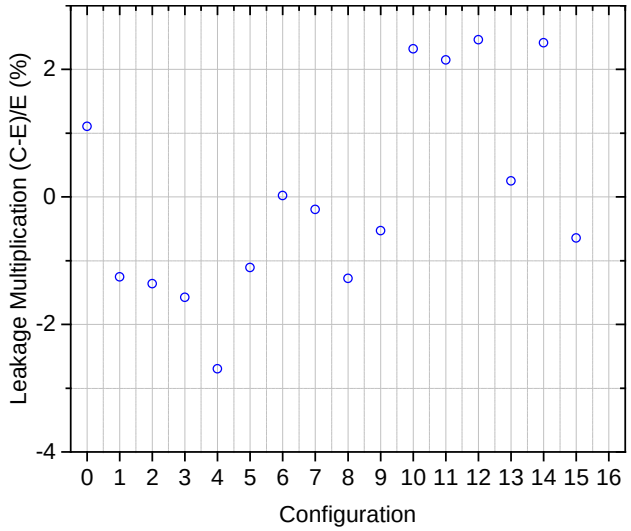

Fig. 17. (C-E)/E comparing IRSN simulated data to measured data.

V. FUTURE WORK

This experiment will be evaluated and documented in an upcoming version of the ICSBEP handbook. This work will help assess the potential impact of this integral measurement as it relates to international efforts to continuously improve current libraries (ENDF, JEFF, JENDL etc…) that still tend to over/under-estimate the measured results of integral experiments, sometimes significantly [14]. Deficiencies in underlying nuclear data quantities such as nubar have been shown to have an effect on inferred values from subcritical measurements as well [15-17]. This experiment and subsequent computational validation will help identify such deficiencies. It will also help validate new nuclear data evaluations, including one for Cu that was recently performed in the resolved region up to 100 MeV for Cu-65 and Cu-63 [18] which is expected to improve Cu-related benchmark simulation performance.

ACKNOWLEDGEMENTS

This work was supported by the Nuclear Criticality Safety Program, funded and managed by the National Nuclear Security Administration for the Department of Energy. This experiment is a joint collaboration with the French Technical Safety Organization (TSO) IRSN.

REFERENCES

1. J. HUTCHINSON, D. LOAIZA, “Plutonium Sphere Reflected by Beryllium,” International Handbook of Evaluated Criticality Safety Benchmark Experiments, NEA/NSC/DOC/(95)03/I, PU-MET-FAST-038.

2. B. RICHARD, J. HUTCHINSON, "Nickel Reflected Plutonium Metal Sphere Subcritical Measurements," International Handbook of Evaluated Criticality Safety Benchmark Experiments, NEA/NSC/DOC/(95)03/I, FUND-NCERC-PU-HE3-MULT-001 (2014).
3. B. RICHARD, et. al., "Tungsten-Reflected Plutonium-Metal-Sphere Subcritical Measurements," International Handbook of Evaluated Criticality Safety Benchmark Experiments, NEA/NSC/DOC/(95)03/I, FUND-NCERC-PU-HE3-MULT-002 (2016).
4. T. CUTLER, et. al., "IER-422: Subcritical Copper-Reflected alpha-phase Plutonium (SCRαP) Integral Experiment," Los Alamos Report LA-UR-16-26285 (2016).
5. J.T. GOORLEY, et. al., "Initial MCNP®6 Release Overview," Nuclear Technology, vol. 180, pp. 298-315 (2012).
6. M. CHADWICK et al. "ENDF/B-VII.1 Nucl. Data for Sci. and Technology: cross sections, covariances, fission product yields and decay data," Nuclear Data Sheets, vol. 112, no. 12, pp. 2887-2996 (2011).
7. J. HUTCHINSON, T. CUTLER "Use of Criticality Eigenvalue Simulations for Subcritical Benchmark Evaluations" Transactions of the ANS Winter Meeting, Las Vegas NV (2016).
8. R. UHRIG, *Random Noise Techniques in Nuclear Reactor Systems*, John Wiley & Sons Inc (1970).
9. J. HUTCHINSON, et. al., "Subcritical Multiplication Experiments & Simulations: Overview and Recent Advances," ANS Advances in Nonproliferation Technology and Policy Conference, Santa Fe NM (2016).
10. A. ROBBA, E. DOWDY, H. ATWATER, "Neutron Multiplication Measurements Using Moments of the Neutron Counting Distribution," Nuc. Instr. and Meth., 215, 473-479 (1983).
11. T. CUTLER, M. SMITH-NELSON, J. HUTCHINSON, "Deciphering the Binning Method Uncertainty in Neutron Multiplicity Measurements," ANS Winter Conference, Anaheim CA (2014).
12. D. CIFARELLI, W. HAGE, "Models for a Three-Parameter Analysis of Neutron Signal Correlation Measurements for Fissile Material Assay," Nuc. Instr. Meth. A251, 550-563 (1986).
13. B. COCHET, et. al., "Capabilities overview of the MORET 5 Monte Carlo code," Joint International Conference on Supercomputing in Nuclear Applications and Monte Carlo 2013 (SNA + MC 2013), La Cité des Sciences et de l'Industrie, Paris, France (2013).
14. S. C. VAN DER MARK, "Benchmarking ENDF/B-VII.1, JENDL-4.0 and JEFF-3.1.1 with MCNP®6," Nuclear Data Sheets, vol. 113, pp. 2935-3005 (2012).
15. E. MILLER, J. MATTINGLY et al. "Simulations of Neutron Multiplicity Measurements with MCNP®-PoliMi," Tech. Rep. SAND2010-6830, Sandia National Laboratory (2010)
16. J. HUTCHINSON, A. SOOD et al. "Comparison of HEU Measurements Using Measured and Simulated Data" Trans. Amer. Nucl. Soc., 106, 487-489 (2013).
17. S. BOLDIN, C. SOLOMON "Simulations of Multiplicity Distributions with Perturbations to Nuclear Data" Trans. Amer. Nucl. Soc., 109, 251-254 (2013).
18. P. PERESLAVTSEVA et al. "New Evaluation of n+63,65Cu Nuclear Cross Section Data up to 200 MeV Neutron Energy" Nuclear Data Sheets, vol. 118, pp. 1-636 (2014).